Available online at www.sciencedirect.com
ScienceDirect
Journal of Bionic Engineering 11 (2014) 541–555

A Bio-Inspired Hopping Kangaroo Robot with an Active Tail

Guan-Horng Liu, Hou-Yi Lin, Huai-Yu Lin, Shao-Tuan Chen, Pei-Chun Lin

Department of Mechanical Engineering, *National Taiwan University*, *Taipei* 106, *Taiwan*

Abstract

Inspired by kangaroo's locomotion, we report on developing a kangaroo-style hopping robot. Unlike bipeds, quadrupeds, or hexapods which alternate the legs for forward locomotion, the kangaroo uses both legs synchronously and generates the forward locomotion by continuous hopping behavior, and the tail actively balances the unwanted angular momentum generated by the leg motion. In this work, we generate the Center of Mass (CoM) locomotion of the robot based on the reduced-order Rolling Spring Loaded Inverted Pendulum (R-SLIP) model, for matching the dynamic behavior of the empirical robot legs. In order to compensate the possible body pitch variation, the robot is equipped with an active tail for pitch variation compensation, emulating the balance mechanism of a kangaroo. The robot is empirically built, and various design issues and strategies are addressed. Finally, the experimental evaluation is executed to validate the performance of the kangaroo-style robot with hopping locomotion.

Keywords: legged robot, kangaroo, hopping, SLIP, tail

Copyright © 2014, Jilin University. Published by Elsevier Limited and Science Press. All rights reserved.
doi: 10.1016/S1672-6529(14)60066-4

1 Introduction

Bio-inspired robotics is a thriving branch of the robotics family. With emulating from nature in mind, robotic researchers try to develop or improve the mechanical structure, mechatronic system, control algorithm, and overall locomotion behavior of the robots by incorporating bio-inspired methodologies. Among all, legged robotics is a particularly popular field of study; not only because the legged form is the morphology adopted by most of ground animals and worth understanding, but also the legged robot has great and obvious potential to initiate dynamic behavior or to negotiate rough terrain.

The study of dynamic robotic systems was initiated by the development of a single-leg hopping robot in the 1980s[1]. Following this, various quadruped and hexapod robots with dynamic behaviors have been reported. For example, the quadruped robot Tekken II has spring-mass-damping systems between the leg joints, as a mechanism to stimulate viscoelastic characteristics of muscle tissue[2,3]. The quadruped robot Scout II can be excited to have dynamically stable bounding gait under complex situation via simple control laws[4,5]. The hexapod Sprawl series has the mixture of active and passive Degree-of Freedoms (DOFs)[6–8], and it can run dynamically with similar motion pattern of the Spring Loaded Inverted Pendulum (SLIP), which is widely recognized as the dynamic model of the running legged animals[9–11]. The hexapod RHex has simple mechanical morphology and control strategy, yet it can perform versatile behaviors[12–16]. Recently the RHex can further perform various interesting dynamic behaviors[17,18]. The RHex also has its amphibious version, Aqua[19], where the proportion mechanism should include the functionality of the leg and fin. The Cheetah robot built at MIT focuses on delicate leg morphology, aiming for high speed running[20]. In addition, various legged robot built by Boston Dynamics Inc (BDI) can possess great mobility, but very limited information is revealed to the public[21]. Besides the quadruped robot and the hexapod robot, the bipedal robot is another popular category of legged robotics. However, maybe owing to challenging stability issue and complex morphology, dynamic running (*i.e.*, with flight phase) of the biped robots is of the least explored and studied area.

Besides the running behavior, hopping or jumping of the legged robots is another popular field. By studying

Corresponding author: Pei-Chun Lin
E-mail: peichunlin@ntu.edu.tw

the morphologies of different frog species, Wang *et al*. constructed a dynamic jumping model based on 4-bar spring/linkage mechanism[22]. Inspired by the dynamical movement of locusts, Chen *et al*.[23] reported on the mechanism and dynamic simulation of the single-bound hopping behavior. Wang *et al*.[24] developed a control algorithm for biped robots by imitating the Central Pattern Generators (CPGs) in hopping or walking animals to equip themselves to unpredictable and changing terrains. The above works are done in theoretical or simulation manner. Some of the works with real robots includes the miniature 7g robot, which can jump much higher than its height by a four-bar linkage with elastic elements and supply power[25]. The robot Grillo also accomplishes continuous jumping by storing elastic energy in a mechanism[26]. The frog robot Mowgli can jump over 50% of its body height by pneumatic muscle actuators[27]. In short, the reported hopping or jumping behaviors on the robot mainly reside on the single stride and large distance jumping, not on the continuous hopping for forward locomotion.

Here, following our initial presentation in Ref. [28], we report on the development of a kangaroo robot with dynamic hopping gait. Though the physical structure of the kangaroos falls in the category of biped animals, the kangaroo legs usually move synchronously. Thus, kangaroo's motion is actually equivalent to a monopod with forward hopping locomotion, a very unique class of motion among the overall legged locomotion. Because the monopods have been studied since 80's, the dynamic hopping behaviors on the empirical platforms have been reported[29], but very limited works relate to the multi-legged robot performing continuous forward hopping locomotion. Or more specifically, the kangaroo-style locomotion is rarely studied. To the best of our knowledge, the only appearance of a kangaroo-style robot is BionicKangaroo designed by FESTO[30], which was announced just after the submission of this paper. This robot has dedicated kangaroo-style legs actuated by a pneumatic actuator. It can hop continuously like a kangaroo, but has lower stride frequency. In contrast, our kangaroo robot has a simplified and template-inspired leg which will be detailed in the next paragraph, while its stride frequency possesses a value comparable to an animal of similar weight.

In this paper we developed dynamic locomotion of the kangaroo robot based on the SLIP-like reduced-order model, R-SLIP model[31], as the "template"[32]. The Center-of-Mass (CoM) trajectory of the robot is set to move according to the passive dynamic trajectory of the R-SLIP model, thus achieving the dynamic motion with minimum effort. Because in reality the robot is a rigid body but not a point mass, the rotational state should be considered for locomotion. Thus, inspired by the kangaroo's morphology, an active tail is implemented for compensating the unwanted angular momentum generated by the legs during locomotion, like the mechanism adopted in kangaroos[33]. The locomotion strategy and control method of the robot is introduced. The robot is empirically built, and pitch balancing experiment and robot hopping experiment are executed.

Recently, the functionality of the tail from the biological aspect has been reported. The tail's role during rapid climbing, aerial descent, and gliding of climbing animals are investigated[34]. The gecko's tail serves as an emergency fifth leg to prevent falling during rapid locomotion with rapid posture change. The research is further carried on to employ a tail on a wheeled robot as a self-righting mechanism[35]. The robot tail functions like the tail of a cat or a gecko, maneuvering the robot posture to prevent crashing from free drop in the air. Following that, the pitch control of the tails in lizards, robots and dinosaurs is investigated, and a unified strategy of the tail-assisted pitch control in all these creatures and the robot is described[36]. Instead of focusing on the aerobatic maneuver as the report work did, our work focuses on the functionality of the tail in ordinary kangaroo-style forward hopping locomotion.

The rest of the paper is organized as follows. Section **2** reviews the bio-inspired robot design process. Section **3** describes the strategy to plan the robot CoM trajectory, and section **4** reports on functionality of the tail on the pitch control. Section **5** briefly describes the mechanism design and mechatronic setup, following by the experimental evaluation and discussion in section **6**. Section **7** concludes the work.

2 Bio-inspired robot design process

In order to design a robot that extracts biological characteristics of a hopping kangaroo, we studied the consecutive side-shot footages of a hopping kangaroo captured by Concord Field Station research team at Harvard University as well as their relevant publication[37], and we performed motion analysis of the foot-

ages. As shown in Fig. 1a, several key positions of the kangaroo were roughly marked for behavioral analysis, including toe (blue rectangle with cross inside), knee (red pentagon), hip (white triangle), pelvis (green rectangle), and tail (yellow star and pink circle). The first four markers were marked by the Concord Field Station, and the last two were added later to the sequential frames. Fig. 1b shows the trajectories of these points during one hopping period of the kangaroo. Because the kangaroo moved forward during side-shooting, the fore-aft position of the kangaroo is determined by tracking accuracy of the recorder, and the fore-aft projections of the trajectories do not correspond to physical movement. Several comments can be draw: (i) The trajectories of hip and pelvis are similar, so the kangaroo body maintains the same posture during locomotion (*i.e*., derivative of pitch is zero). If kangaroo body is treated as a rigid body, CoM of the kangaroo is expected to have similar trajectory. (ii) The body, leg, and tail of the kangaroo exhibit periodic motions, and all are with the same period. The CoM also has one vertical up-down cycle in one stride. This behavior is similar to the running of legged animals, whose motion can be approximated by the SLIP model[9], including the kangaroo[38]. (iii) The leg and tail move in the same frequency but in the opposite directions, so the angular momentums generated by these two motions can be alleviated. In addition, the other videos also reveal that the motions of two legs are closely synchronized for forward hopping. So, as with other reduced-DOF modeling work, the two legs can be treated as one "virtual leg" moving in the sagittal plane. Based on these observations, we obtain the following bio-inspired principles for designing a kangaroo robot. (i) The robot body can be approximated by a rigid body, and it has no pitch variation during locomotion. (ii) The tail is acted as a balancing mechanism to even out the angular momentum caused by the swing legs during robot locomotion. Though the kangaroo exhibits a more complex motion pattern in tail movement as shown in Fig. 1b, for balancing purposes the robot's tail can be approximated by an actively-movable rigid body. This design also simplifies the follow-up model derivation and control. (iii) The robot should be designed to have bilateral symmetry, and the legs are set to move synchronously. (iv) Because of bilateral symmetry, the planar model in sagittal plane is sufficient for analyzing forward hopping locomotion of the robot. In

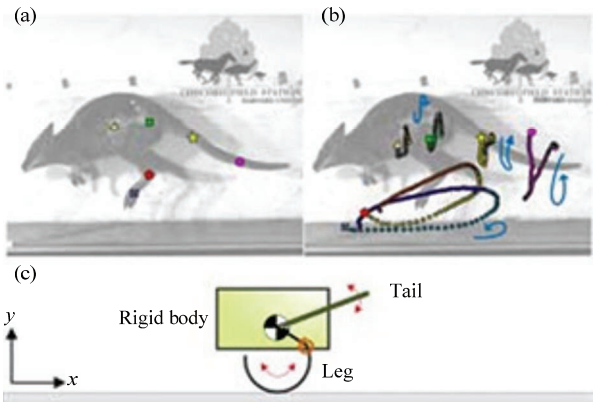

Fig. 1 A side-shot of a hopping tammar wallaby captured by Concord Field Station research team at Harvard University. (a) Key positions for motion analysis; (b) trajectories of these positions during a single hopping stride; (c) simple sagittal-plane model of the hopping robot. Image courtesy of Concord Field Station at Harvard University.

that case, the roll, yaw, and later displacement of the robot's spatial motion can be ignored, and only the states of fore-aft displacement, vertical displacement, and pitch are preserved in the modeling work.

Following the setup described in the last paragraph, one important and undetermined issue is the locomotion model of the robot. Alexander suggested that animal legs exhibit elastic behavior like a spring[9]. Later, Blickhan conducted further analysis of running and hopping motion by a spring-mass model[10]. After the initiation, the SLIP model has been widely used as the reduced-order "template" of dynamic legged locomotion[32]. Thus, the leg should be excited to have compliant behavior during locomotion. Instead of actively controlling a multi-DOF leg to act like a passive spring (*i.e*., like a kangaroo), a passive spring is directly used as the empirical robot leg to simplify mechanical and mechatronic infrastructure[39], which can be called a template-inspired leg morphology. However, direct implementation of SLIP-like spring as the legs may not be practical owing to the following reasons. (i) It is indeed challenge to design and fabricate an ideal massless linear spring with enough stiffness to resist lateral external force. This force is crucial because it drives the robot body forward, especially when the robot's motion is intended to have dramatically change or in fast running. (ii) The ideal point-contact of the leg to the ground is not suitable for practical implementation because the friction force is most-likely not sufficient to support dramatic load for forward motion. Note that animals have feet and/or

claws to support the ground traction, and this feature is not captured by the SLIP model. As a result, following the morphology of RHex which uses half-circular material as the compliant legs[40,41], here the thin circular-shape fiberglass is utilized as the leg as shown in Fig. 2b. Hereafter it is referred to as the circular leg. The length of the circular arc is extended to be more than one half-circle, allowing rolling behavior and avoiding point-contact behavior[42]. However, though the circular leg can be regarded as the massless and compliant leg, it has two distinct performance characteristics which differ from the ideal linear spring. First, the linear spring ideally has a fixed ground contact point, in contrast to the circular leg which rolls on the ground so that the ground contact point keeps moving forward. The second difference is that, owing to the forward movement of the ground contact point, equivalent linear stiffness of the circular leg changes as it rolls on the ground. As a result, the linear spring utilized in the SLIP model may not be able to represent the behavior of the circular legs. Our previous study showed that the virtual leg of rolling SLIP (R-SLIP) model shown in Fig. 2a is a good model for the compliant circular leg[31]. As a result, R-SLIP model is utilized as the template for the CoM locomotion of the robot.

Several study results have helped us overcome the issues of scaling and CoM positioning. Heglund *et al*. reported that the stride frequencies of the animals are a function of their weight[43]. Dickinson *et al*. reported that animals with different sizes have different leg stiffness in order to fit their respective moving velocities[44]. Their results allow us to calculate the leg stiffness of the hopping robot with the designated size and weight. Alexander *et al*. performed various measurements regarding the force exerted by the kangaroo during the hopping motion[33], and the free body diagram analysis reveals that the axes of the legs and the tail are approximately coincided. In the one legged hopping robot designed by Zeglin, the axes are also coincided, easier in control and even mass distribution[45]. With this arrangement, the body pitch change caused by gravity in the flight phase can be reduced. As a result, the robot is designed, or as close as possible, to have the CoM and two rotational joints located at the same point in the view of sagittal plane.

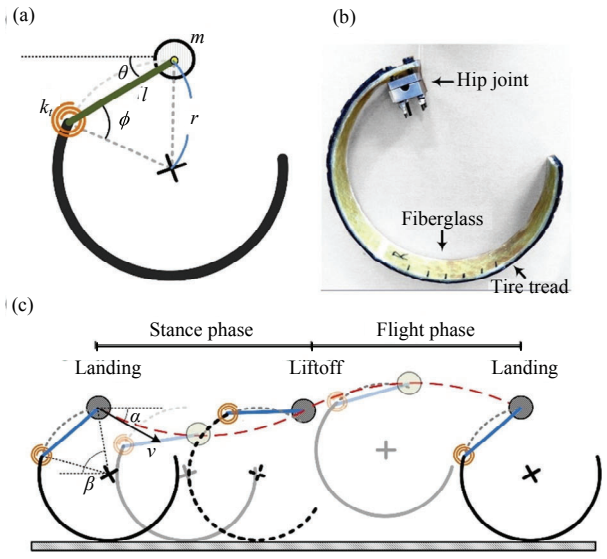

Fig. 2 The characteristics of R-SLIP model: (a) The four intrinsic parameters r, k_t, m, l; (b) the circular leg of the robot; (c) dynamic motion of the R-SLIP model in one stride. Three Initial Conditions (ICs) at touchdown moment α, β, v are also shown.

With the design decisions described in this section, the morphology of the robot in the sagittal plane is sketched in Fig. 1c. The design of the hopping robot obeys the physical conditions and movements of the kangaroo in terms of synchronized leg motion, leg compliance, relative motion of the tail and the leg, fixed body posture, physical arrangement of the tail and the leg, *etc*. In addition, the spatial motion of the real robot is simplified to planar motion in the sagittal plane.

3 Dynamic motion of the robot CoM

Because the R-SLIP model[31] serves as the reduced-order "template" of the original complex "anchor," the planar motion of the kangaroo robot[32] as shown in Fig. 2c is utilized to develop the robot's dynamic locomotion. The R-SLIP model is used as the guidance for robot's 2-dimensional translational motion, and the remaining 1-dimensional rotational pitch motion is controlled separately and will be described in section **4**. The mapping of robot's translational motion to the R-SLIP model is quite straight forward. The motion of robot CoM corresponds to that of the R-SLIP's point mass according to Newtonian Dynamics. The motion of the robot's compliant circular legs should be driven to act like a single "virtual" spring of the R-SLIP model. Though the virtual leg of the R-SLIP model may not be able to completely extract the dynamic behavior of the circular leg, it is so far the best reduced-order model for the compliant circular material.

The characteristics of the R-SLIP model are briefly

described as follows. As shown in Fig. 2a, it comprises two parts: the bottom part is a rigid circular rim, and the upper part is a linear rod. Both parts are massless, and they are connected by a torsional spring. Thus, the R-SLIP has four intrinsic parameters: the radius of the circular rim (r), the stiffness of the torsional spring (k_t), mass (m), and the distance between the torsion spring and the mass (l). Dynamic motion of the R-SLIP model is composed of two phases as shown in Fig. 2c: Stance phase, where the leg of the model is in contact with the ground, and flight phase, where the model is in ballistic flight. During the stance phase, the torsional spring is compressed and stores the potential energy, functioning like the tendon of the kangaroo. When the torsional spring recovers back, the stored potential energy changes back into kinetic energy, providing power for the model to enter the ballistic flight phase. In the flight phase, gravity is the only external force acting on the model, and the dynamic behavior follows the projectile equation. At the moment that R-SLIP model lands on the ground, the flight phase ends, and the next stance phase of the model starts. The dynamic equations of the model can be solved by Lagrangian method, and detailed derivation can be found in Ref. [31]. With four preset system parameters (r, k_t, m, l) and chosen ICs, the system dynamics in a full stride can be numerically evaluated. The ICs of the model are given at the moment of touchdown (*i.e*., beginning of the stance phase), which includes landing angle (β), touchdown speed (v), and touchdown angle included by the touchdown velocity and horizontal line (α) as shown in Fig. 2c.

To successfully use R-SLIP as the template of the robot, the parameters of the model should be matched to the robot specifications. Thus, the dynamic behavior of the model has better chance to be excited on the robot. The robot mass is treated known, and then the leg stiffness is selected based on the relationship between the stiffness of the leg and animal body mass reported in Ref. [46]. Next, the hopping frequency is roughly estimated based on mice-to-horse curve[43], where Ref. [47] has more details. With the mass, the leg property and other geometrical dimensions of the robot, the four intrinsic parameters of the R-SLIP model (r, k_t, m, l) can be computed. Table 1 lists the values of the model parameters for analysis.

Stable running trajectory of the R-SLIP model is selected based on the return map analysis[31]. As shown in Fig. 3a, the fixed point exists when the next $(i+1)^{\text{th}}$ touchdown angle (α_{i+1}) is the same as the current i^{th} touchdown angle (α_i). Moreover, the fixed point is stable when its slope is between 1 and −1. Otherwise it is considered as an unstable fix point. Fig. 3b plots the distribution of the fixed points within the range if ICs are achievable by the empirical robot. Ideally, if the robot is operated near or at the stable fixed points, it moves like the R-SLIP model, and it can stably run without any energy input (*i.e*., purely passive dynamics). However, in practical the robot is not energy conservative due to various energy loss terms such as friction and damping, so the motor power is required to drive the "virtual leg" and provides the energy input to the system, so the energy level of the robot can be kept unchanged. Considering stability and empirical motor power rating, v =1.5 m·s^{-1} and α = 44° are chosen as the ICs of the robot. Following this, stance-phase time 0.145 s, flight-phase time 0.186 s, and lift-off angle 11.52° can be yielded. The solved mass trajectory of the R-SLIP is implemented as the ideal CoM trajectory of the robot, which also equals to the leg trajectory $\theta(t)$. The motion is highly nonlinear, so it is solved off-line and is approximated by a fifth-order polynomial. The approximated and the original trajectories are plotted in Fig. 4. The Root Mean Square Error (RMSE) between these two trajectories is 0.0181°, showing that the polynomial approximation matches the original trajectory quite well. The leg trajectory during the flight phase can be freely designed as long as it satisfies the speed and profile continuity. The algorithm of leg trajectory generation is also shown as a sub-algorithm of the overall control system in Fig. 5.

Table 1 Variables list

R-SLIP model				Tail dynamic model							
m (kg)	r (m)	k_t (N·m)	l (m)	m_b (kg)	m_l (kg)	m_t (kg)	r_b (m)	θ_b (°)	r_l (m)	r_{th} (m)	r_{tv} (m)
5.400	0.100	16.2	0.118	4.606	0.423	0.371	0.017	55.0	0.090	0.120	0.177

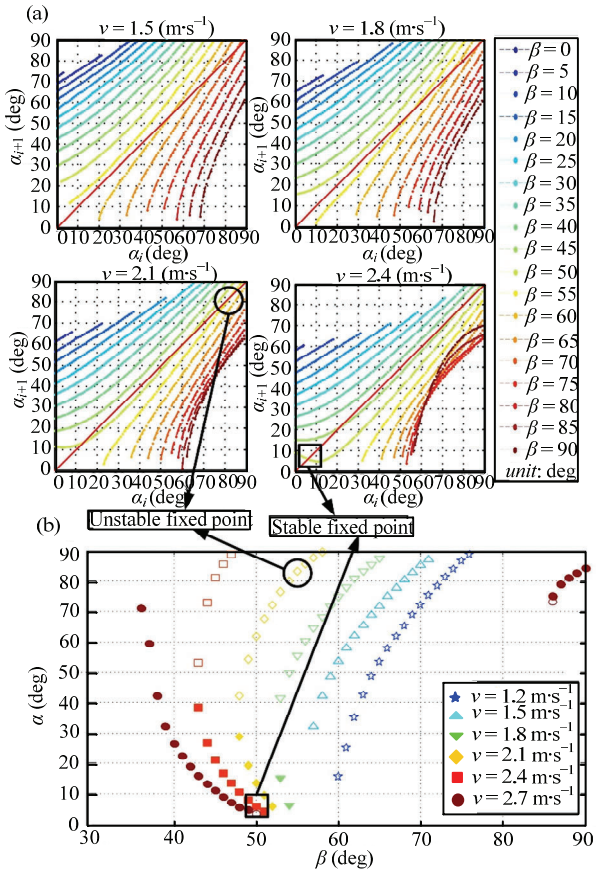

Fig. 3 Stability analysis of the R-SLIP model: (a) Return map and (b) distribution of the stable and unstable fixed points. The symbols β, α, and v indicate the landing angle, touchdown angle, and touchdown speed, respectively. The filled and hollow legends represent stable and unstable fixed points, accordingly.

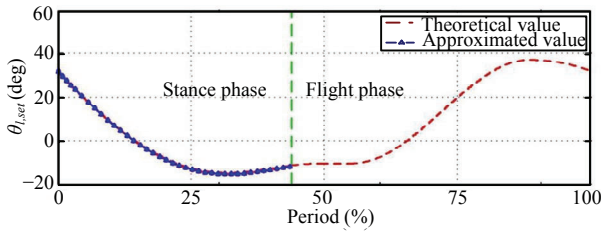

Fig. 4 The ideal leg trajectory of the robot, shown in dashed red. The blue curve with triangular markers is the approximated trajectory implemented on the robot. θ_l represents the leg position, which will be further defined in Fig. 6. The ICs are v = 1.5 m·s^{-1}, α = 44°and β = 58°. The hopping period is 0.33 s.

4 Robot tail motion

The body pitch should be regulated to maintain at the desired value, so the deployed leg trajectory can drive the robot to match the mass motion of the R-SLIP model. Based on the bio-inspired process described in section **2**, an active tail is chosen as the pitch regulation mechanism. The regulation mechanism is mainly active while the robot is in its flight phase. While the robot in its stance phase, ideally the robot moves purely by passive dynamics without motor input, and in that situation no external torque is generated to alter the body orientation. In contrast, while the robot is in its flight phase, the motor power should be applied to repose the legs back to the ICs for the next touchdown. The torque applied to the legs generates unwanted reactive torque back to the robot and make the body pitch change. In addition, relative movements of the legs and the tail to the body also cause the variation of the CoM position. When the CoM of the overall robot does not locate at the rotation axis (*i.e.*, hip joint), where the leg is mounted, the gravity will also generate another unwanted torque to make the body pitch change. Thus, the motion of the tail is designed to compensate for the effects caused by these two factors. This compensation mechanism requires a dynamic model of the overall robot, including the body, leg, and tail.

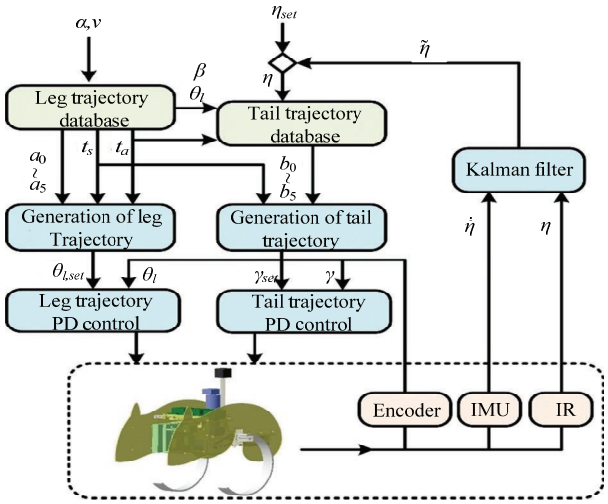

Fig. 5 Control strategy of the hopping robot.

The derivation of the dynamic model is described as follows. Fig. 6 plots the notations for the model development. While the robot is in its flight phase, the moment equation can be expressed as

$$-gm_l r_l \sin(\theta_l + \eta - \delta_l) - gm_b r_b \cos(\eta + \delta_b) + gm_t(r_{th} + r_{tv}\sin(\eta + \gamma)) = I_b\ddot{\eta} + I_l(\ddot{\theta}_l + \ddot{\eta}) + I_t(\ddot{\gamma} + \ddot{\eta}). \quad (1)$$

By importing the ICs of these states, the tail trajectory can be solved numerically. The values of the geometric parameters for solving Eq. (1) are listed in Table 1. Because Eq. (1) is also highly nonlinear, the trajectory of the robot tail is solved off-line and is approximated by a fifth-order polynomial function. The trajectories with

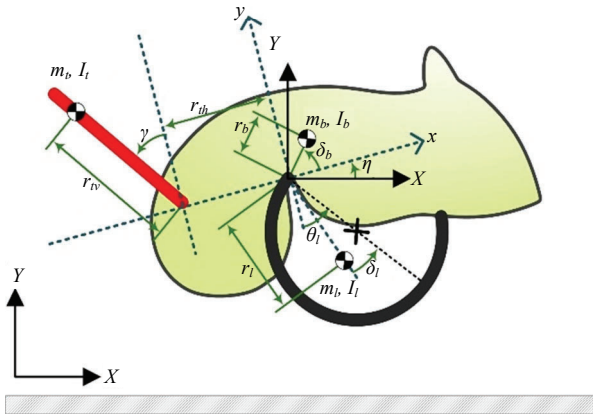

Fig. 6 Sketch of the robot model in sagittal plane. The symbols for dynamic equation derivation are also plotted. The body, the leg, and the tail have masses m and inertias I. The subscripts b, l and t indicate the body, the leg, and the tail, accordingly. The symbols θ_l and γ are the orientations of the leg and the tail in the body frame, respectively. The symbol η represents the body pitch, defined as the angle included by the x-axes of the world frame and the body frame. The parameters r_b, δ_b, r_l, δ_l and r_{lv} are introduced to define the relative CoM configurations of the body, the leg, and the tail with respect to the body frame.

various possible sets of the ICs are computed and stored as the database. The robot controller selects one of the trajectories in the database to generate the tail trajectory of the robot in its flight phase. Fig. 7 shows the nominal trajectory as the example, where body pitch and pitch rate are both zeroes. The figure shows both the approximated and the original trajectories. The RMSE between these two trajectories is 1.9004e−04, showing that the polynomial approximation matches the original trajectory quite well. The algorithm of tail trajectory generation described in this section is also shown as a sub-algorithm of the overall control system in Fig. 5.

The quantitative presentation of the robot tail model shown in Eq. (1) reveals that the tail trajectory is affected by the leg trajectory during flight phase as well as the undesired body pitch when the robot lifts off. The

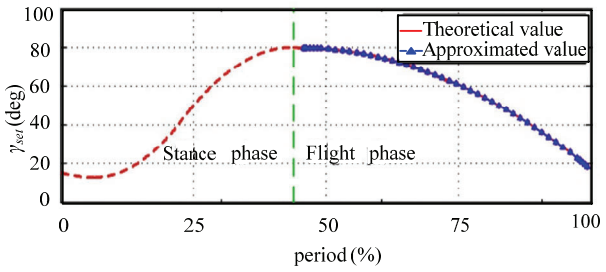

Fig. 7 The ideal tail trajectory of the robot, shown in dashed red. The blue curve with triangular markers is the approximated trajectory implemented on the robot.

former effect can be further calculated by the flight-phase time and the landing as well as lift-off posture of the robot leg. Therefore, the tail trajectory is affected by four variables: flight-phase time (t_a), leg landing angle (β), leg lift-off angle (θ_l), and lift-off body pitch (η). Generally, the first three variables are automatically determined while the R-SLIP model with specific ICs is selected. Therefore, they can be quantitatively derived from the database described in section **3**. The last parameter, body pitch, can be either manually set to a desired value (*i.e*., open-loop method) or estimated by an onboard state estimator (*i.e*., closed-loop method). With all four parameters determined, the tail trajectory can be quantitatively generated.

The body pitch η of the robot is estimated by the Kalman Filter (KF)[15,48] with two sensory inputs: Infrared Rangers (IR) and a gyro. The two infrared rangers are placed on the front and back sides of the robot to measure the distance from the body to the ground. The body pitch can then be simply calculated by trigonometric relation of the body to the ground. The gyro provides the body pitch rate. By fusing these two signals into the KF, the estimated body pitch can have fast response and free from accumulated integration error. The quantitative formulation of the body pitch estimator is described as follows. In the time update, the constant acceleration model is utilized, and jerk is treated as the noise source. In the measurement update, the body pitch derived from the IR sensors and the body pitch rate as measured by the gyro are imported. The detailed process is similar to our previous work in Ref. [15]. The structure of the body pitch estimator is also included in Fig. 5.

5 Robot design and mechatronic infrastructure

Design of the kangaroo robot basically follows the planar model structure described in section **3** and **4**, and several empirical design issues should be considered to grant the model structure is realizable on the real robot. (i) The first issue is the dimension discrepancy, where the model is planar and the robot is a spatial object. The robot is designed in a lateral symmetric manner just like a real kangaroo. The legs are placed symmetrically with respect to the sagittal plane, and the tail is located on that plane. The legs and the tail move in the planes paralleled or in the sagittal plane, and the legs are set to move synchronically. The CoM is arranged to locate in the

sagittal plane and close to the hip joint, achieved by adjusting the positions of the components on the robot body. The empirical CoM position of the robot is measured by placing the robot on the 6-axis force plate in two different orientations. In each placement, the force plate yields the projected position of the robot's center of gravity. By extending these projected positions in the directions orthogonal to the force plate, the CoM can be found where the positions intersect. (ii) The second issue is the driving system of the robot. Though the present work only focuses on the forward motion of the robot and in this case the legs can indeed be driven by one motor owing to the synchronous leg motion, two motors are adopted to independently drive two legs in the final design, which preserves the possibility of implementing the turning mechanism in the future by applying different leg configurations. Synchronizing the motion of two legs is achieved by the leg position control, and the performance was empirically validated before the experimental data analysis. (iii) The third issue is the limited available space around the CoM. The rotational axes of the tail and two legs should be coincident at the same point in the sagittal plane model, and the final mechanism arrangement is shown in Figs. 8a and 8b. The motor driving the tail is vertically installed and connected to the tail through a bevel gear pair. The motors driving the legs are installed parallel to the leg rotation axis, and the kinetic energy is transmitted to the legs through the pulley-and-belt systems. (iv) The fourth issue is the nominal configuration of the tail. Instead of using the horizontal posture as the nominal configuration as the kangaroo does, the nominal tail configuration is oriented up to provide a wider operational range without colliding to the ground during robot locomotion. (v) The fifth issue is the materials of the robot. The robot body is made of commercial fiberglass composites, which is lightweight, high strength, and non-conductive. On the other hand, the fiberglass legs are custom-made by ourselves, so the stiffness can be tuned to the desired value. The photo of the leg is shown in Fig. 2b.

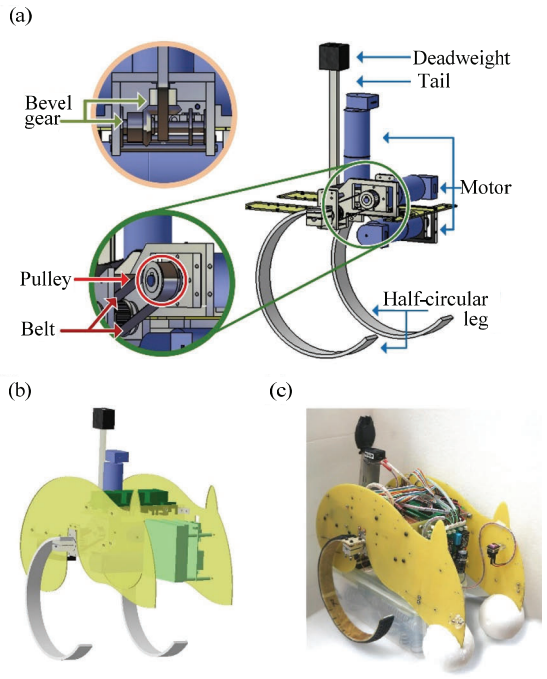

Fig. 8 The kangaroo robot: (a) CAD drawing which shows transmission system of the robot; (b) the CAD drawing of the robot; (c) the photo of the robot.

The mechatronic system of the robot is briefly introduced as follows. The robot has a real-time embedded control system (sbRIO-9606, National Instruments) running at 500 Hz loop rate, accompanying with an integrated Field Programmable Gate Array (FPGA) for high-speed non-floating algorithm computation and I/O signal exchange, such as D I/O for logic commands, analog-to-digital converter (ADC, MCP3208, Microchip) for analog sensors, pulse width modulation (PWM) for DC motor control, and SPI interface for inertial measurement unit (IMU) readings. The sensors include a six-axis IMU (ADIS16364, Analog Devices) mounted at the CoM for pitch rate measurement, two IR rangers (GP2Y3A001K0F, Sharp) for pitch determination, two hall-effect sensors (42A, Honeywell) for leg configuration calibration, one photo interrupter (CNZ1023-DN, Panasonic) for tail motion calibration and electronic stops. The remote operator communicates with the robot via 802.11b wireless standard, and this communication channel is used for high-level motion commanding and robot status monitoring. The robot weighs 5.4 kg and the dimension is 0.46 m in length, 0.265 m in width, 0.24 m in height. Figs. 8b and 8c show a CAD drawing and a photo of the robot.

6 Experimental results and discussion

Two sets of experiments are conducted for performance validation: one is for evaluating the tail performance, and the other is for evaluating the robot hopping motion. For the latter experiment, the motion of the robot is computed based on the sequential snapshots taken by a stationary camcorder (HDR-SR11, Sony)

from side view. Four LEDs are mounted on the robot head, rotational axis of the legs *(i.e.*, CoM), tail end, and leg toe. Thus, by deriving the positions of the markers in the image frame, the planar states of the robot versus time can be computed, including forward and vertical CoM displacements and body pitch. The leg and tail motions relative to the body can be obtained as well. The force interaction of the robot to the ground is measured by a six-axis force plate (FP4060−07, Bertec), and the forward and vertical forces are extracted for analysis. A median filter with a window size 20 is applied to smooth the raw force measurement data.

6.1 Performance of the tail on body pitch balancing

Prior to the robot hopping experiments, the functionality of the tail on body pitch balancing is evaluated. Fig. 9 shows the experiment setup, including the schematic drawing and the photo of the empirical setup. The robot is hung in the air, free from the effect and disturbance coming from the force interaction between the robot and the ground. In addition, the robot is hung by two wires at its hip joints (*i.e.*, at the CoM in the sagittal plane model), so the pitch DOF is not constrained and the gravity effect can be minimized. The experimental setup is similar to the setting of tail motion derivation shown in section **4**; thus, the tail balancing mechanism derived based on the conservation of angular momentum can be experimentally evaluated. During the experiments, the legs move forward and backward periodically and reciprocally, and the tail is programmed to move in three different modes: no movement (*i.e.*, stationary tail), movement without sensory input *(i.e.*, fixed tail trajectory, open-loop mode), and movement with body pitch sensory input (*i.e.*, closed-loop mode). In the open-loop mode, the nominal tail trajectory is utilized. On the other hand, in the closed-loop mode, the controller selects the adequate trajectory based on the sensory inputs.

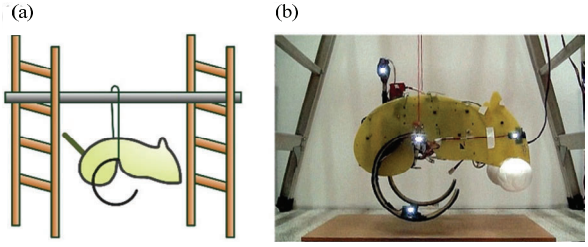

Fig. 9 The setup for tail-assisted body pitch balancing: (a) Schematic drawing; (b) the photo of the setup.

Table 2 Statistical results of body pitch variations

Methods	RMS error	Max range
Stationary tail	2.24˚	7.18˚
Active tail with open-loop mode	1.17˚	5.27˚
Active tail with closed-loop mode	0.96˚	4.49˚

Table 2 lists the statistical results of this experiment with 8 runs, where the RMSEs and the maximum movement ranges (*i.e.*, maximum body pitch minus minimum body pitch during experiment) of the body pitch are reported. The results show clearly body pitch variation decreases while the tail-assisted balancing mechanism is implemented. With the open-loop active tail, the body pitch RMSE of the robot reduces close to 52% in comparison to the robot with non-active tail. With the closed-loop active tail, the value is further down to 43%. In comparison to the open-loop mode, the closed-loop mode improves 18%, not as significant as the change from non-active tail to the active tail. The maximum ranges of body pitch have similar trend as well.

6.2 Performance of the robot with hopping locomotion

The robot is programmed to perform hopping locomotion based on the strategy described in section **3** and **4**. The stable hopping motion composed of the stance phase and the flight phase are depicted in Fig. 10a, and Fig. 10b is the snapshot extracted from one of the experiment run. The present work focuses on the stable hopping locomotion of the real robot; thus, having right ICs for the robot to initiate its periodic stable locomotion is essential to evaluate the validity of the methodology proposed in the paper. The ICs include states of the planar rigid body

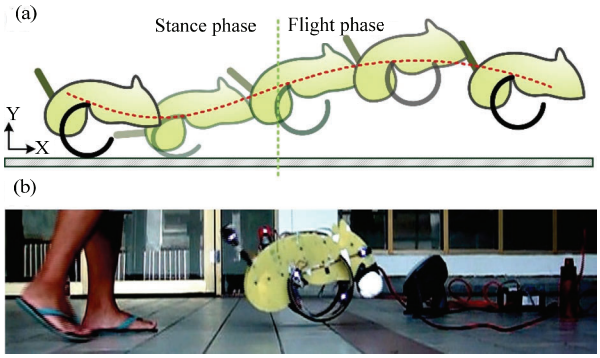

Fig. 10 The kangaroo robot with hopping locomotion. (a) Schematic drawing of the robot with hopping locomotion in one period; (b) snapshot of the hopping robot.

system, such as CoM touchdown velocity, CoM touchdown angle, leg configuration, body pitch, body pitch rate, *etc*. Empirical experience on robot experiment runs reveals that it is very hard to provide correct ICs in all states to the robot by merely throwing the robot to the ground by an operator or by a sliding guide system. Through trial-and-error process we found that the feasible solution of providing roughly adequate ICs to the robot is gradual transition from vertical hopping to forward hopping. At the very beginning, the robot is supported by four thin wires at four corners of the body, which roughly defines and confines the configuration of the robot at rest. Then the robot is set to hop. Because of the wires, the robot can move freely in the vertical direction but constrained in the forward direction. During the hopping motion the wires keep at the same configuration, so when the robot lands on the ground, the body pitch can be regulated to the right value. In the meantime, the operator also gradually moves forward to reduce the forward motion constraint to the robot. After about six transition strides, the robot can roughly reach the desired ICs. Because of using this state transition method, the images shown in Fig. 10b has human operator following the robot. It is not perfect but at least applicable to the hopping experiment.

The quantitative results of the robot with hopping locomotion are shown in Figs. 11 and 12. Fig. 11 shows the CoM displacement of the robot versus time in

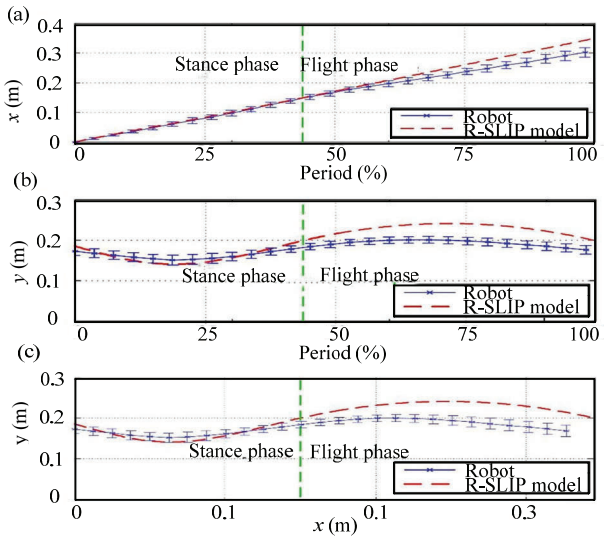

Fig. 11 Hopping trajectory of the robot (blue curve, with mean (middle blue curves) and standard deviation (std, top and bottom blue bars)) and the R-SLIP model (red dashed curve). (a) Horizontal CoM trajectory (x) versus normalized time; (b) vertical CoM trajectory (y) versus normalized time; (c) planar CoM trajectory.

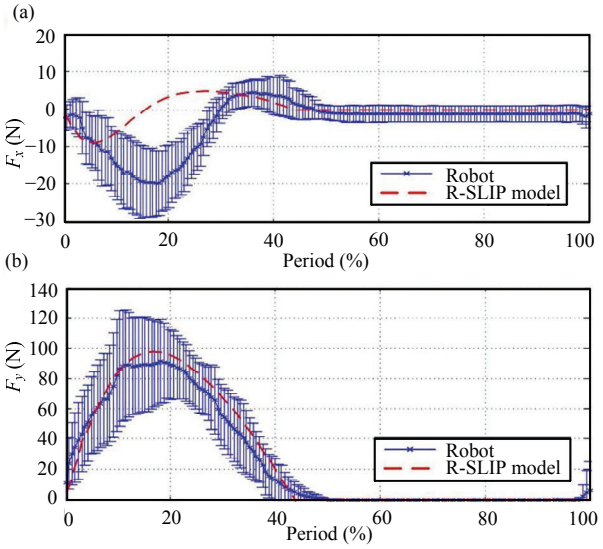

Fig. 12 The forward (F_x) and vertical (F_y) ground reaction forces of the robot (blue curve, with mean (middle blue curves) and standard deviation (std, top and bottom blue bars)) and the R-SLIP model (red dashed curves) during stance phase.

Figs. 11a and 11b and its sagittal-plane trajectory in Fig. 11c. For comparison purpose, the ideal CoM trajectories derived from the R-SLIP model are also plotted (red dashed curves). The figure shows that the CoM trajectory of the empirical robot in stance phase matches that of the R-SLIP model in the reasonable manner, but that in the flight phase has larger discrepancy. Fig. 12 shows the forward and vertical ground reaction forces of the robot versus time, where the horizontal axis is normalized by the stride period.

Fig. 12 shows that the vertical ground reaction force of the robot matches quite well to that of the R-SLIP model, but the forward ground reaction force has some inconsistencies between these two. We believe the discrepancy mainly resulted from operating point change and un-modeled characteristics of the robot. We observed that the actual touchdown angle α of the robot in the experiments is about 20°–25°, different with the setting value α = 44°. As a result, the leg spring compression level of the robot is less than that of the R-SLIP model, so the ballistic trajectory of the robot CoM is not as high and as long as that of the R-SLIP model. In addition, the empirical leg is a continuously compliant leg, whose behavior is much more complicated than the virtual leg of the R-SLIP model. Finally as a side note, the CoM displacement of the robot in the flight phase is also underestimated by about 20% owing to the definition of the CoM position. On the empirical robot the

marker representing the CoM is mounted fixedly on the body, but the actual robot CoM moves when the leg and tail move, which causes positioning error of 1 cm – 2 cm between the CoM computed by marker and the actual one. This phenomenon is also observed on the animal locomotion experiments[49].

Fig. 13 plots the body pitch of the robot versus time in a complete hopping stride. The figure reveals that the body pitch tends to be positive during the whole hopping stride. When the robot moves forward without sufficient ICs forward velocity, the leg actuation according to the ideal R-SLIP trajectory will make the body pitch up and has less forward displacement as planned. In consequence, in the next touchdown the landing angle of the robot with positive body pitch decreases, and the leg ground contact point shifts closer to the leg rotation axis (*i.e*., hip joint), yielding a lower compression of the leg than the desired value in the stance phase. The lower compression of the leg limits the transformation from initial kinetic energy to potential energy, which increases the forward velocity and meantime decreases the vertical velocity in the stance phase. The decrease of vertical velocity yields the less flight height in comparison to that of the R-SLIP model, which matches the trends shown in Fig. 11b. In addition, the decreased landing angle of the robot also yields a longer deceleration period in its stance phase because the leg takes longer time to pass the vertical posture for acceleration. The phenomenon described above also explains why the state transition method can be used to gradually make the robot hop forward. During the transition process, though the body pitches up, the forward velocity gradually increases to the desired ICs value.

To further understand the behavior of the R-SLIP model with different ICs as well as to investigate the discrepancy between the model behavior and the robot behavior, the effects of ICs on the mass trajectory and ground reaction forces are plotted in Fig. 14. The effect of changing touchdown angle α is shown in Fig. 14(a–c). When α increases, the robot tends to jump higher, and this trend explains the in-sufficient robot hopping height in comparison with the model as shown in Fig. 11. When α increases, the robot hits the ground with higher impact force and causes higher ground reaction force in the stance phase. Though the higher ground reaction force decelerates the horizontal velocity, it helps the kinetic energy to be stored into elastic potential energy and then results in larger vertical ground reaction forces as shown in Fig. 14c. It is worth noting that when α keeps increasing, the momentum of the robot for going forward decreases, the forward ground reaction force may not follow the standard pattern of "decelerate and then accelerate" as shown in Fig. 14b with $\alpha = 60^{\circ}$. In the extreme case, the robot may decelerate, stop, and then go backward, ceasing the periodic motion. The effect of changing β is shown in Fig. 14(d–f). In contrary to the effect of changing α, when β increases, the robot tends to hop lower but longer. When the robot enters the stance phase with higher β, the leg is easier to roll through central line of the leg and then starts accelerating forward. This behavior increases the rolling length of the leg on ground, resulting in longer period of stance phase as well as higher horizontal velocity of the robot when it enters the flight phase. Meanwhile, it also causes less compression of the leg and thus lowers the vertical velocity, which is shown in the lower maximum value of vertical ground reaction force in Fig. 14f. In addition, when β is too small, the robot can rarely accelerate forward as shown in the red line of Fig. 14e, which indicates that the robot tends to jump vertically but not moving forward.

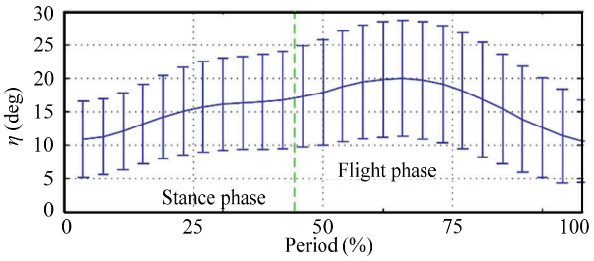

Fig. 13 The body pitch angle verses normalized time. Mean (middle blue curve) and standard deviation (std, top and bottom blue bars) are reported.

The imperfect setting of the empirical system or the disturbance may lead the behavior of the robot deviate from the planned one. The motors are driven based on the passive dynamic of the R-SLIP model. When the robot lands with the right conditions, the passive dynamics of the robot lets the robot move just like the R-SLIP model. In this case, the hip joints act like a free joint and the motors do not contribute to the leg motion. In contrast, when the setup is not ideal, the motors generate torques, driving the legs to follow the planned trajectory versus time. In this case, the generated torque to the leg also creates a reactive torque to the body in the

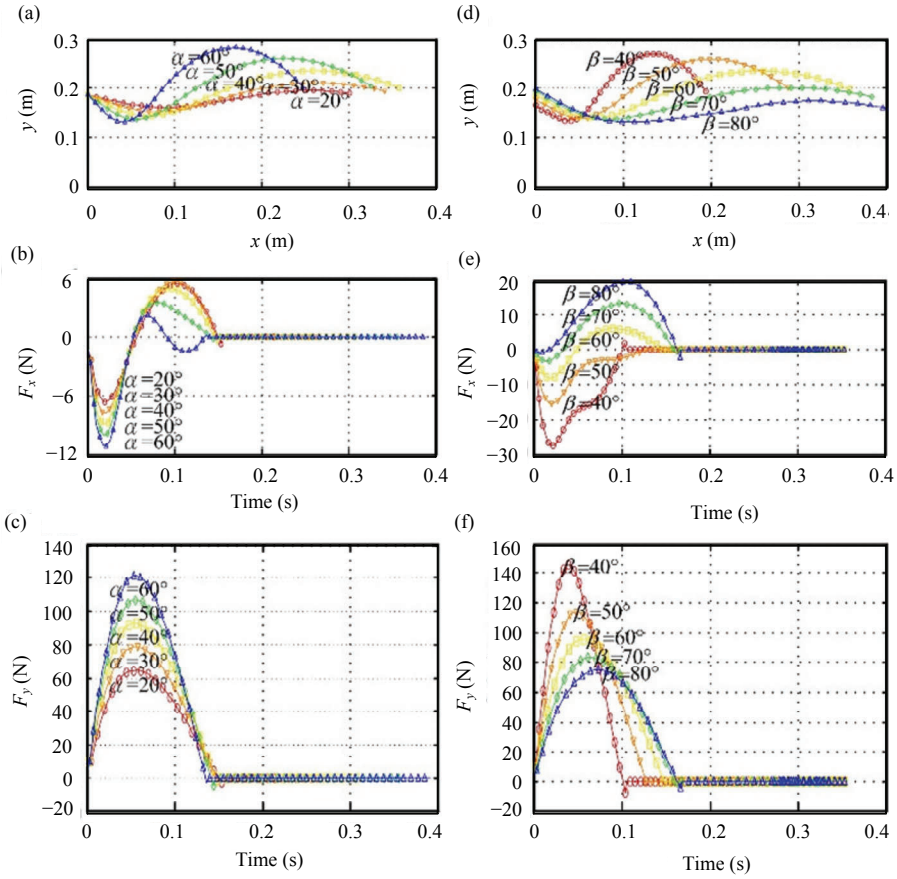

Fig. 14 The mass trajectory and the ground reaction forces of the R-SLIP model with (a–c) varying touchdown angle and $\beta = 58^\circ$ as well as with (d–f) varying landing angle and $\alpha = 44^\circ$. The touchdown velocity is $v = 1.5$ m·s^{-1}.

opposite direction, which makes the body pitch up. Because some discrepancy exists between the robot and the model (such as leg mass and complex circular leg behavior), the pitch-up phenomenon is observed in the experiments as shown in Fig. 13. With this undesired and gradually-increased body pitch, the robot fails to hop after several strides. As a result, the tentative solution to remedy this accumulated error is to use the mounted wires to calibrate the body pitch back to the consistent condition at the lift-off moment. By carefully checked the sequential images recorded by the camcorder, we confirm that the strings interferes with the system about 20% time in each stride, which made the experimental setup not perfect but tolerable. With this calibration, the robot could hop continuously. Though several imperfect conditions exist in current methodology, the use of R-SLIP model as the motion template[32] for the robot still plays an important role of developing the robot with dynamic behavior. If the robot doesn't have compliant legs, it is hard to initiate the dynamics. The leg with ideal linear spring behavior is also hard to be found, and empirically we found that the half-circular leg is the feasible solution. Owing to this empirical constraint, the R-SLIP model is the adequate model to use, and this approach allows us to quickly initiate the dynamics of the robot, with some detailed quantitative difference between them.

The experimental results shown in the previous paragraphs are extracted from the data when the robot uses open-loop method. The tail-assistive strategy is functional because the robot without active tail cannot hop. However, we also found that though the robot with closed-loop method performs slightly better than that with open-loop method in the balancing experiment shown in subsection **6.1**, the robot with closed-loop method didn't hop well in the forward hopping experiment. Without the sensory system and algorithm which detect the exact moments of landing and taking-off, the response of active tail actually aggravates the compensate mechanism toward instability. The aggressive tail

motion also makes it easily out of its working range. This causes collision between the tail to the body or the ground, and the accompanied impact makes the hopping motion unstable. In summary, the robot with closed-loop method is inherently prone to locomotion instability. A better closed-loop strategy would require the development of a real-time full body state estimator which correctly captures the real motion of the robot as well as a complete multi-body dynamic model that is applicable to both ground phase and flight phase which allows us to nurture the compensation mechanism. This work is nontrivial and is currently under investigation, and it will be reported separately. In the current stage, the robot with open-loop active tail is the adequate solution owing to its functional yet simple infrastructure.

7 Conclusion

We report on the development of a kangaroo robot with dynamic locomotion. The use of the R-SLIP model helps in the morphology design of the robot as well as initiating its dynamic hopping behavior. The experimental result shows that the robot with the active tail can significantly reduce the body pitch variation to about half in comparison to the robot with the stationary tail. In comparison with the open-loop active tail, the closed-loop active tail can further improve the performance but not as significant as from stationary tail to active tail. The second experiment reveals that it is a challenge to transit the robot from a stationary state to the designed stable locomotion. Once transient, the robot can hop for a couple of strides without being tethered. The accumulated body pitch error is the main cause for the robot to fail on long time-scale hopping, and this deviation also induces the tail motion to gradually shift its operation region from middle to one side of its achievable motion range. This reveals the facts that the robot in this configuration may not have wide stable region, and the carefully-tuned operation point and the whole-body model may be required for further motion improvement. Though not perfect, the current design morphology of the robot allows the robot to induce the dynamic locomotion of the kangaroo robot, which clearly exhibits the alternating behavior of stance phase and flight phase.

We are currently working on revising the mechatronic system of the robot, which can provide more accurate sensory information and stronger computation power. Thus a more sophisticate closed-loop strategy of tail motion can be implemented. We are also investigating the possibility of implementing the whole body dynamic model, which would allow us to design the transition from stationary to stable hopping, thus achieving a more robust 3-dimensional and un-tethered hopping locomotion.

Acknowledgment

The authors would like to thank Chun-Kai Huang for discussing the development issues in mathematical modeling, sensor developing, and programming. This work is supported by National Science Council (NSC), Taiwan, under contract NSC 100-2628-E-002-021-MY3.

References

[1] Raibert M H. *Legged Robots That Balance*, MIT Press, Cambridge, MA, 2000.

[2] Kimura H, Fukuoka Y, Cohen A H. Adaptive dynamic walking of a quadruped robot on natural ground based on biological concepts. *International Journal of Robotics Research*, 2007, **26**, 475–490.

[3] Fukuoka Y, Kimura H, Cohen A H. Adaptive dynamic walking of a quadruped robot on irregular terrain based on biological concepts. *International Journal of Robotics Research*, 2003, **22**, 187–202.

[4] Poulakakis I, Smith J A, Buehler M. Modeling and experiments of untethered quadrupedal running with a bounding gait: The Scout II robot. *International Journal of Robotics Research*, 2005, **24**, 239–256.

[5] Poulakakis I, Papadopoulos E, Buehler M. On the stability of the passive dynamics of quadrupedal running with a bounding gait. *International Journal of Robotics Research*, 2006, **25**, 669–685.

[6] Kim S, Clark J E, Cutkosky M R. iSprawl: Design and tuning for high-speed autonomous open-loop running. *International Journal of Robotics Research*, 2006, **25**, 903–912.

[7] Cham J G, Karpick J K, Cutkosky M R. Stride period adaptation of a biomimetic running hexapod. *International Journal of Robotics Research*, 2004, **23**, 141–153.

[8] Cham J G, Bailey S A, Clark J E, Full R J, Cutkosky M R. Fast and robust: Hexapedal robots via shape deposition manufacturing. *International Journal of Robotics Research*, 2002, **21**, 869–882.

[9] Alexander R M. *Elastic Mechanisms in Animal Movement*, Cambridge University Press, Cambridge, England, 1988.

[10] Blickhan R. The spring mass model for running and hopping.

Journal of Biomechanics, 1989, **22**, 1217–1227.

[11] Yu H, Li M, Wang P, Cai H. Approximate perturbation stance map of the SLIP runner and application to locomotion control. *Journal of Bionic Engineering*, 2012, **9**, 411–422.

[12] Saranli U, Buehler M, Koditschek D E. RHex: A simple and highly mobile hexapod robot. *International Journal of Robotics Research*, 2001, **20**, 616–631.

[13] Altendorfer R, Moore N, Komsuolu H, Buehler M, Brown H B, McMordie D, Saranli U, Full R, Koditschek D E. RHex: A biologically inspired hexapod runner. *Autonomous Robots*, 2001, **11**, 207–213.

[14] Lin P C, Komsuoglu H, Koditschek D E. A leg configuration measurement system for full-body pose estimates in a hexapod robot. *IEEE Transactions on Robotics*, 2005, **21**, 778–778.

[15] Lin P C, Komsuoglu H, Koditschek D E. Sensor data fusion for body state estimation in a hexapod robot with dynamical gaits. *IEEE Transactions on Robotics*, 2006, **22**, 932–943,.

[16] Chou Y C, Yu W S, Huang K J, Lin P C. Bio-inspired step-climbing in a hexapod robot. *Bioinspiration and Biomimetics*, 2012, **7**, 036008.

[17] Johnson A M, Koditschek D E. Toward a vocabulary of legged leaping. *IEEE International Conference on Robotics and Automation* (*ICRA*), 2013, 2553–2560.

[18] Chou Y C, Huang K J, Yu W S, Lin P C. Design of leaping behavior in a planar model with three compliant and rolling legs. *Proceedings of the 16th International Conference on Climbing and Walking Robots and the Support Technologies for Mobile Machines*, Sydney, Australia, 2013, 479–486.

[19] Prahacs C, Saudners A, Smith M K, McMordie D, Buehler M. Towards legged amphibious mobile robotics. *Proceedings of the Canadian Engineering Education Association*, 2011.

[20] Ananthanarayanan A, Azadi M, Kim S. Towards a bio-inspired leg design for high-speed running. *Bioinspiration & Biomimetics*, 2012, **7**, 046005.

[21] Playter R, Buehler M, Raibert M. *BigDog*. In: Proceedings of SPIE, San Jose, USA, 2006, **6230**, 62302O.

[22] Wang M, Zang X Z, Fan J Z, Zhao J. Biological jumping mechanism analysis and modeling for frog robot. *Journal of Bionic Engineering*, 2008, **5**, 181–188.

[23] Chen D, Yin J, Zhao K, Zheng W, Wang T. Bionic mechanism and kinematics analysis of hopping robot inspired by locust jumping. *Journal of Bionic Engineering*, 2011, **8**, 429–439.

[24] Wang T, Guo W, Li M, Zha F, Sun L. CPG control for biped hopping robot in unpredictable environment. *Journal of Bionic Engineering*, 2012, **9**, 29–38.

[25] Kovac M, Fuchs M, Guignard A, Zufferey J C, Floreano D, . A miniature 7g jumping robot. *IEEE International Conference on Robotics and Automation*, Pasadena, CA, 2008, 373–378.

[26] Li F, Liu W T, Fu X, Bonsignori G, Scarfogliero U, C Stefanini, Dario P. Jumping like an insect: Design and dynamic optimization of a jumping mini robot based on bio-mimetic inspiration. *Mechatronics*, 2012, 22, 167–176.

[27] Niiyama R, Nagakubo A, Kuniyoshi Y. Mowgli: A bipedal jumping and landing robot with an artificial musculoskeletal system. *IEEE International Conference on Robotics and Automation* (*ICRA*), Roma, Italy, 2007, 2546–2551.

[28] Liu G H, Lin H Y, Lin H Y, Chen S T, Lin P C. Design of a kangaroo robot with dynamic jogging locomotion. *IEEE/SICE International Symposium on System Integration*, Kobe, Japan, 2013.

[29] Sayyad A, Seth B, Seshu P. Single-legged hopping robotics research-A review. *Robotica*, 2007, **25**, 587–613.

[30] FESTO. BionicKangaroo-energy-efficient jump kinematics based on a natural model. 2014, http://www.festo.com/cms/en_corp/13704.htm.

[31] Huang K J, Lin P C. Rolling SLIP: A model for running locomotion with rolling contact. *IEEE/ASME International Conference on Advanced Intelligent Mechatronics* (*AIM*), Kachsiung, Taiwan, 2012, 21–26.

[32] Full R J, Koditschek D E. Templates and anchors: Neuromechanical hypotheses of legged locomotion on land. *Journal of Experimental Biology*, 1999, **202**, 3325–3332.

[33] Alexander R, Vernon A. The mechanics of hopping by kangaroos (Macropodidae). *Journal of Zoology*, 1975. **177**, 265–303.

[34] Jusufi A, Goldman D I, Revzen S, Full R J. Active tails enhance arboreal acrobatics in geckos. *Proceedings of the National Academy of Sciences*, 2008, **105**, 4215–4219.

[35] Chang-Siu E, Libby T, Tomizuka M, Full R J. A lizard-inspired active tail enables rapid maneuvers and dynamic stabilization in a terrestrial robot. *IEEE/RSJ International Conference on Intelligent Robots and Systems* (*IROS*), San Francisco, CA, 2011, 1887–1894.

[36] Libby T, Moore T Y, Chang-Siu E, Li D, Cohen D J, Jusufi A, Full R J. Tail-assisted pitch control in lizards, robots and dinosaurs. *Nature*, 2012, **481**, 181–184.

[37] McGowan C P, Baudinette R V, Usherwood J, Biewener A. The mechanics of jumping versus steady hopping in yellow-footed rock wallabies. *Journal of experimental biology*, 2005, **208**, 2741–2751.

[38] McMahon T A, Cheng G C.The mechanics of running: how does stiffness couple with speed? *Journal of Biomechanics*,

1990, **23**, 65–78.

[39] Zhou X, Bi S. A survey of bio-inspired compliant legged robot designs. *Bioinspiration & Biomimetics*, 2012, **7**, 041001.

[40] Moore E Z. *Leg Design and Stair Climbing Control for the RHex Robotic Hexapod*, Master's thesis, Department of Mechanical Engineering, McGill University, 2002.

[41] Lin P C. *Proprioceptive Sensing for a Legged Robot*, PhD thesis, University of Michigan, 2005.

[42] Chen S C, Huang K J, Chen W H, Shen S Y, Li C H, Lin P C. Quattroped: A leg-wheel transformable robot. *IEEE/ASME Transactions on Mechatronics*, Taipei, Taiwan, 2013.

[43] Heglund N C, Taylor C R, McMahon T A. Scaling stride frequency and gait to animal size: Mice to horses. *Science*, 1974, **186**, 1112–1113.

[44] Dickinson M H, Farley C T, Full R J, Koehl M A R, Kram R, Lehman S. How animals move: An integrative view. *Science*, 2000, **288**, 100–106.

[45] Zeglin G J. *Uniroo-A One Legged Dynamic Hopping Robot*, Bachelor's thesis, Department of Mechanical Engineering, Massachusetts Institute of Technology, 1991.

[46] Farley C T, Glasheen J, McMahon T A. Running springs-speed and animal size. *Journal of Experimental Biology*, 1993, **185**, 71–86.

[47] Huang K J, Chen S C, Lin P C. A bio-inspired single-motor-driven hexapod robot with dynamical gaits. *IEEE/ASME International Conference on Advanced Intelligent Mechatronics* (*AIM*), Kaohsiung, Taiwan, 2012.

[48] Kalman R E. A new approach to linear filtering and prediction problems. *Transactions of the ASME-Journal of Basic Engineering*, 1960, **82**, 35–45.

[49] Heglund N, Cavagna G, Taylor C. Energetics and mechanics of terrestrial locomotion. III. Energy changes of the centre of mass as a function of speed and body size in birds and mammals. *Journal of Experimental Biology*, 1982, **97**, 41–56.